Molecular Crystals and Liquid Crystals

Publication details, including instructions for authors and subscription information:
http://www.tandfonline.com/loi/gmcl20

Optical Phase Modulation Using Dual-Frequency Nematic Liquid Crystals

Mikhail I. Barnik [a], Artur R. Geivandov [a], Vladimir V. Lazarev [a], Serguei P. Palto [a] & Serguei V. Yakovlev [a]

[a] Shubnikov Institute of Crystallography of Russian Academy of Sciences, Moscow, Russia

Version of record first published: 22 Sep 2010

To cite this article: Mikhail I. Barnik, Artur R. Geivandov, Vladimir V. Lazarev, Serguei P. Palto & Serguei V. Yakovlev (2008): Optical Phase Modulation Using Dual-Frequency Nematic Liquid Crystals, Molecular Crystals and Liquid Crystals, 480:1, 49-71

To link to this article: http://dx.doi.org/10.1080/15421400701821606

Mol. Cryst. Liq. Cryst., Vol. 480, pp. 49–71, 2008

ISSN: 1542-1406 print/1563-5287 online
DOI: 10.1080/15421400701821606

Optical Phase Modulation Using Dual-Frequency Nematic Liquid Crystals

Mikhail I. Barnik, Artur R. Geivandov, Vladimir V. Lazarev, Serguei P. Palto, Serguei V. Yakovlev
Shubnikov Institute of Crystallography of Russian Academy of Sciences, Moscow, Russia

Phase modulation characteristics of dual-frequency liquid crystal materials possessing the dielectric anisotropy sign inversion have been studied in detail under the quasi-static and dynamic electric field control. It was found that the main obstacle in development of dual-frequency liquid crystal modulators having simultaneously short response time and large switchable values of phase retardation is related to an electrohydrodynamic instability, which disturbs the director reorientation. We are discussing general conditions at which a stable 2π phase modulation is possible at highest switching frequencies. In particular, for the developed dual-frequency liquid crystal material we have established conditions at which the stable phase retardation dynamic range of 2π at switching time ~ 2 ms is realized at room temperature.

Keywords: adaptive optics; dual-frequency liquid crystal; phase retardation

1. INTRODUCTION

There are many examples of electrically addressable liquid crystal (LC) phase modulators (LCPMs) used in adaptive optics systems for the wave-front controllers, see [1–14] for instance. The idea of an LCPM device is based on an electrically controlled LC director field distortion that results in a change of optical phase retardation for the light passing through an LC layer. Nematic liquid crystals (NLCs) are most frequently used for LCPM devices.

The work was supported by CRDF (GAP) under Project RPO-1411-MO-03.
Address correspondence to Mikhail I. Barnik, Shubnikov Institute of Crystallography of Russian Academy of Sciences, Leninskii pr.59, 119333 Moscow, Russia. E-mail: lcl@ns.crys.ras.ru

A simplified version of LCPM represents a LC cell, which consists of two parallel sided plate substrates (made, for instance, of glass) with a thin gap between them. The inner surfaces of substrates are successively covered by transparent electrodes and alignment layers. The thin gap of the cell is filled with LC, and alignment layers provide a desired LC director field distribution in a field-off state. For NLC materials with a positive dielectric anisotropy $\varepsilon_a = \varepsilon_{||} - \varepsilon_{\perp}$($\varepsilon_{||}$ and $\varepsilon_{\perp}$ are dielectric permittivities along and perpendicular to the LC director, respectively), if a driving field is applied along the normal to a planarly aligned LC layer, the director (local optical axis) tends to be oriented along the electric field vector. At an electric field large enough the LC director becomes along the normal almost over a whole cell thickness, so the LC optical axis is getting perpendicular to the plane of an LC layer. When an applied voltage is switched off, the LC director field relaxes to its initial state.

Due to a large value of LC birefringence $\Delta n = n_e - n_o$ (n_e and n_o are extraordinary and ordinary refractive indices of NLC for light polarized parallel and perpendicular to LC director orientation, respectively), which can reach a value of ~ 0.3 and higher, a change in an optical phase retardation $\Delta\Phi$ of several π can be obtained at an LC layer thickness d of a few micrometers. For example, $\Delta\Phi = 2\pi \cdot \Delta n \cdot d/\lambda \approx 8\pi$ for red laser light ($\lambda = 0.633\,\mu\text{m}$) passing layer of a thickness $d = 8\,\mu\text{m}$ of NLC with $\Delta n = 0.3$.

A switching-on time characterizing the director reorientation to a new equilibrium state, and consequently the time of phase retardation change, at presence of an electric field E can be estimated as $\tau_{\text{on}} \sim \gamma/(E^2 \varepsilon_0 \varepsilon_a)$. For typical value of NCL rotational viscosity $\gamma \sim 0.1\,\text{Pa}$ ($\varepsilon_0 \approx 8.85 \times 10^{-12}\,\text{F/m}$) the values τ_{on} less than 0.1ms can be achieved at a moderate electric field strength of $E = U/d = 5\,\text{V}/\mu\text{m}$. The further decrease of τ_{on} is possible at an increase of the voltage U.

An essential drawback of nematic LCPM devices is a slow relaxation time τ_{off} to an initial field-off state after a driving voltage is switched off ($\tau_{\text{off}} \sim \gamma \cdot d^2/(\pi^2 K)$). For known up-to-date least viscous NLCs at a typical value of effective elastic constant $K \sim 10\,\text{pN}$ the time τ_{off} is of about 20 ms at $d \sim 5\,\mu\text{m}$. The latter relaxation time can be decreased by lowering the LC layer thickness. However, at a desired 2π value of the phase modulation (for a true correction of a light wave front distortion a phase modulator device has to provide a gradual control in the change of an optical phase retardation not less than 2π) the lowest thickness is limited by LC birefringence.

NLC materials of a special type, so called dual-frequency liquid crystal materials (2f-LCMs), allow increasing the operational speed of LCPM devices [15–20]. Such 2f-LCMs have a positive dielectric

anisotropy at low electric field frequencies and negative anisotropy at the high frequencies. The fast response time in this case can be achieved by active (field-on) control of switching to different optical states. For example, an initial planar LC director configuration is switched to homeotropic one, when the low frequency (LC has a positive dielectric anisotropy at this frequency) voltage is applied to a cell. Then, the homeotropic LC texture can be switched back to the planar state by applying the high frequency field, which interacts with the negative dielectric anisotropy.

There are many examples of 2f-LCMs applications for phase modulation of light [21–26]. However, detailed investigations of phase modulator properties have not been done till now. It is known at the same time that the phase switching is complicated by many undesirable processes. For instance, under dual-frequency mode of operation, complicated multidomain director field configurations can be induced by back flow streams [17] that, of course, complicate the controllable phase modulation. As the most advanced investigation, it should be emphasized the works of researches of the Kent State University team [27,28]. Therein a dual-frequency mode of operation have been investigated for specific case of the initial (field-off) LC orientation, when LC is homogeneously aligned with a director pretilt at $\Theta \sim 45^\circ$ with respect to the substrate plates of the cell. The authors of [27] claimed very fast switching of a net optical retardation of 0.3–2.2 μm during a time interval of 150–500 μs. However, from their experimental data one can not unambiguously conclude that they indeed have obtained the claimed dynamic range of the phase retardation change. From the data in [27,28] it is clearly seen that the 100% light intensity modulation was not observed for a particular experimental geometry studied. The latter means that the light polarization state was not changed in a desired manner to provide necessary phase retardation. Our computer simulations show that the back-flows are developing and EHD instability appears under the conditions the authors used. It is important to mention that the influence of the back flow on a director field distribution during dual-frequency driving was studied in works [29,30]. In [29], for instance, the director tilt angle distribution in a hybrid LC cell has been reconstructed from optical measurements made with leaky guided-mode technique. The authors pointed out an inversion of director tilt sign close to the homeotropic surface (Fig. 3(b) in Ref. [29]) and correctly explained this by back flow effects. However, therein (in Ref. [29]) a rather "soft" driving regime was used, when relatively low driving voltage ($V_{pp} = 20\,V$) at low dielectric anisotropy ($\Delta\varepsilon(2\,kHz) = +2$ and $\Delta\varepsilon(60\,kHz) = -1$) was providing switching on a long time scale of 10 ms. For this reason the

authors where not able to see that the back flow effect can be developed into instabilities, which provide principal limitations on switching speed in dual-frequency LCs.

In this work we have investigated the modulated phase characteristics of 2f-LCMs in quasi-static and dynamic regimes. We point out a principal role of EHD resulting in limitations of speed and value of phase modulation. To our mind, the appearance of EHD instability is a general property characteristic of dual-frequency materials. Taking it into account allows optimizing switching parameters of LCPM devices. As an example we are demonstrating a possibility of stable 2π phase retardation dynamic range switching for time ~ 2 ms.

2. 2f-LCM DEVELOPMENT AND ELECTRO-OPTIC INVESTIGATION TECHNIQUE

A. Dual-Frequency Liquid Crystals Materials Development

Our approach to development of 2f-LCMs is based on established correlations of dipole relaxation dynamics and LCs molecular structure [31]. An essential part of the developed 2f-LCMs is low polarity two-benzene-ring nematic compounds. The positive dielectric anisotropy of LCMs at low frequency $f_{LF} < f_i$ (f_i is the frequency of dielectric anisotropy sign inversion) is provided using polar LC additives with a high longitudinal dipole moment of molecules. The molecules of these LCs should contain at least three benzene rings separated by "bridges" to achieve the dipole relaxation in lowest sound frequency range. The dielectric anisotropy at high frequencies $f_{HF} > f_i$ is controlled by two-ring LC molecules with a large lateral dipole moment. Same principle has been used by one of the authors (M.I.B) for development of known LC-1001 material, which is often used in dual-frequency experiments [22,23].

Supposing that by variation of viscous-elastic 2f-LCM characteristics the EHD instability can greatly be suppressed, or, at least, the value of its threshold voltage can be increased, we have developed series of mixtures based on LC materials combination of different chemical classes such as azoxybenzene derivatives, esters, acetylene derivatives (tolanes), dicyano-derivatives of esters and salicylidenes. Unfortunately, we have found that the EHD instability exists and provides approximately the same limitations for the phase retardation switching in all the developed materials. Based on these experimental results and computer simulations we came to a conclusion that the problem is general. One can not escape of the EHD instability, while some improvements are possible with increasing values of $|\alpha_2/\alpha_4|$ and $|\alpha_2/\alpha_5|$, where α_i are Leslie viscosity coefficients.

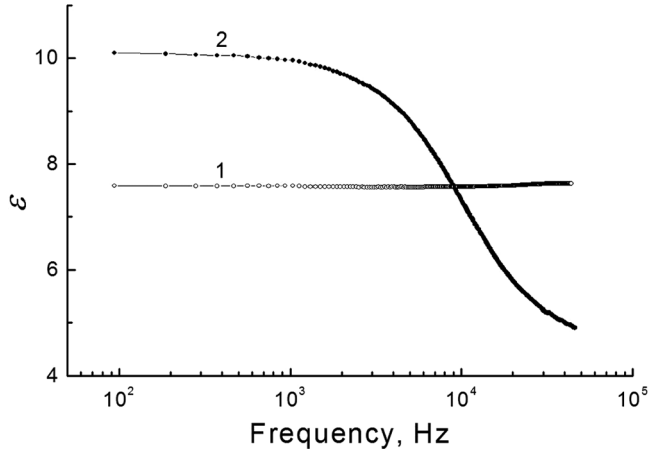

FIGURE 1 Spectral dependencies of principal components of dielectric permittivities $\varepsilon_{\perp}(1)$ and $\varepsilon_{||}(2)$ for the AP-99-1 dual-frequency mixture at $T = 21^{\circ}C$.

All experimental data presented here were received with 2f-LCM called AP-99-1. These results reflect principal features of switching also observed for the other developed LCs. The mixture AP-99-1 is characterized by following physical parameters at room temperature ($T = 21^{\circ}C$): $\varepsilon_a(1\,kHz) = 2.4$, $\varepsilon_a(40\,kHz) = -2.6$, $f_i = 9\,kHz$, $\Delta n = 0.25$, $K_1 = 9.7\,pN$, $K_3 = 16.5\,pN$. The temperatures of phase transitions are following: from nematic to smectic $T_{NS} = <-7^{\circ}C$ and from isotropic to nematic $T_{I-N} = 74^{\circ}C$ at cooling and from nematic to isotropic $T_{N-I} = 78^{\circ}C$ at heating. The dielectric spectra of AP-99-1 mixture are shown in Figure 1. Dielectric constants $\varepsilon_{\perp}$ and $\varepsilon_{||}$ were measured in the planar and homeotropic cells, respectively, using the dielectric Fourier-spectrometer of the PhysLab software providing a set of different "virtual devices" also (oscilloscope, arbitrary waveform generator, a lock-in amplifier, and some others).

B. Experimental Technique of Electro-Optical Investigations

The electro-optical investigations were made with cells providing two different types of initial LC director field distribution. The difference between cells is explained with a reference to Figure 2. The angular orientation of the director in a fixed *xyz* laboratory frame at the top inner surface of the cell in Figure 2(a) is the same as that at the bottom inner surface. Further a cell of such a director arrangement referred to as a cell of homogeneous alignment, or a 0-aligned cell. The other

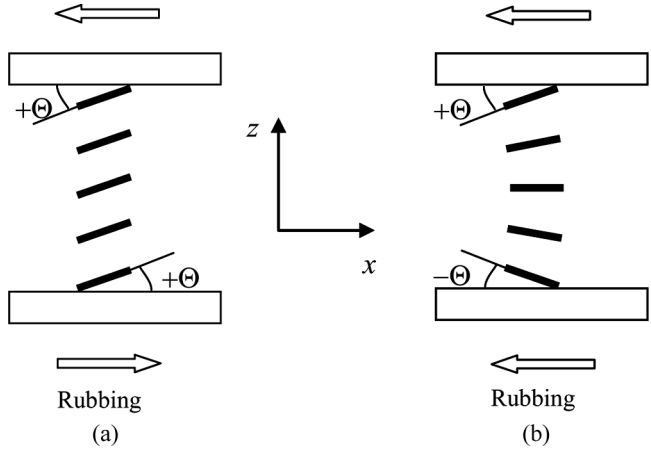

FIGURE 2 Schematic representation of 0-aligned (a) and π-aligned (b) cells (no voltage applied).

director arrangement is shown in Figure 2(b): therein the director pretilt angle at the counter surfaces is of opposite sign. The opposite pretilt direction is equivalent to 180° rotation of the director and such cell will be named "π-aligned" cells. For 0-aligned cells the director field is uniform throughout the thickness of LC layer, but for π-aligned cells the director field has a splay distortion. In both cases the LC director arrangement was controlled by rubbing of the polyimide alignment layers that gives a pretilt angle of $|\Theta| \sim 3$–4° [32].

In quasi-static electro-optical measurements the rate of voltage step-wise amplitude growing on LC cells was of about 0.1 V/s. Thus the LC director field distribution was corresponding to equilibrium state at each value of the effective voltage. The sinusoidal voltage of 1 kHz frequency was used. An experimental set-up (see Fig. 3), based on an ellipsometric principle [33], was used for measurements of the electro-optical response, optical anisotropy and optical phase retardation in quasi-static mode of operation. A beam of a He–Ne laser (2 mW, $\lambda = 633$ nm) is split by plate (S) for signal (1) and the reference (2) beams. The signal beam linearly polarised by a polarizer (P) with axis at 45° to the vertical passes through a LC sample, $\lambda/4$-plate (QP) and then is modulated by a rotating polarizer playing a role of analyser (RA). The reference beam, also linearly polarised in the same direction, passes the same rotating analyser. Two identical silicon photodiodes (PDS and PDR) detect the modulated optical signals and deliver electric response signals to a two-channel line input of a

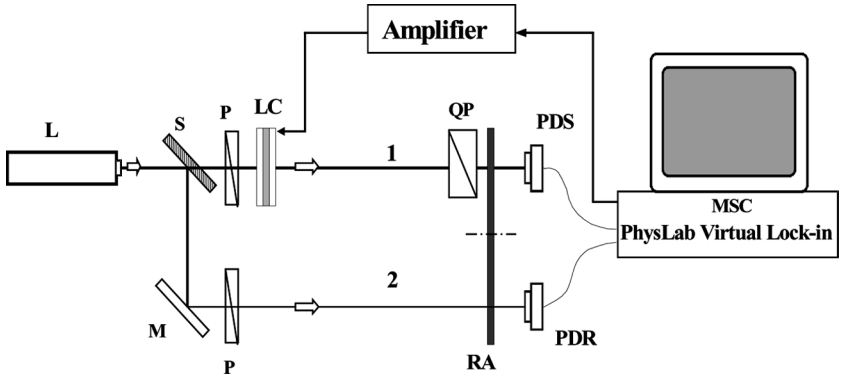

FIGURE 3 Scheme of ellipsometric set-up for electro-optical investigations. He–Ne laser (**L**), beam splitter (**S**), mirror (**M**), polarizers (**P**), liquid crystal cell (**LC**), $\lambda/4$-plate (**QP**), rotating analyzer (**RA**), photodiodes (**PDR** and **PDS**) in reference (**1**) and signal (**2**) channels, multimedia sound card (**MSC**) of the computer.

multimedia sound card (MSC) of the computer. The PhysLab software was used for LC voltage driving and for automated measurements of a phase shift between electric responses of the reference and signal channels. For this set-up geometry the phase shift between the two signals measured by virtual Lock-In equals exactly to the optical phase retardation $\Delta\Phi$ for the two orthogonally polarised waves propagating in LC media. The effective birefringence Δn_{eff} of the LC layers was estimated from the expression $\Delta n_{\text{eff}} = \lambda\Delta\Phi/(2\pi d)$.

In the dynamic experiments the electro-optical response has been investigated using the dual-frequency modulated pulse packets consisting of a sequence of low frequency (1 kHz) square-waveform pulse and high frequency (35 kHz) sinusoidal waves. The scheme of set-up for studying electro-optical properties of LCs in dynamic mode of operation is shown in Figure 4. The set-up is assembled on base of polarizing microscope "POLAM-113" produced by LOMO corporation (Russia). LC cells are placed between microscope polarizers on the microscope stage. Light beam from He–Ne laser ($\lambda = 633$ nm) passed through the microscope optical system and a LC cell is registered by a photomultiplier and oscilloscope "Tektronix3012" connected to a computer. The driving voltage is synthesized by PhysLab virtual arbitrary waveform generator and after additional amplification is applied to the LC cell. The microscope system also gives a possibility for a visual inspection of the studied LC cells owing to a prism of total reflection being inserted into the microscope optical scheme.

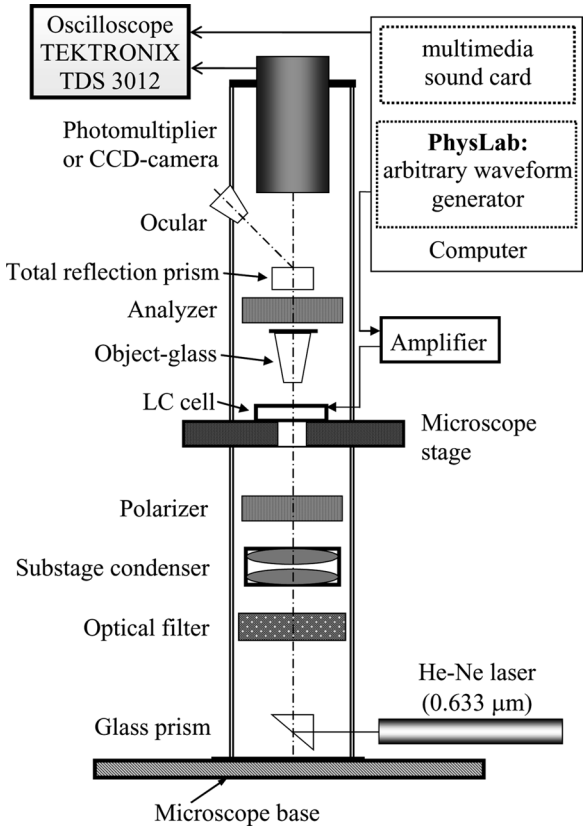

FIGURE 4 Microscope-based experimental set-up for electro-optical investigations.

"Panasonic WV-CL700/G" CCTV camera connected to the computer was optionally installed into the microscope instead of the photomultiplier that allows imaging and saving the LC textures.

To study the thickness dependency of electro-optical characteristics, wedge-cells were assembled of two 1 cm in thickness, 1.5 cm in width and 7.5 cm in length of a size glass plates. Due to large thickness of glass plates the gap thickness in wedge-cells was gradually variable from zero to 20 μm. One of the inner surfaces was covered with a solid electrode, while the other had a system of 2.5 mm in width parallel electrode stripes spaced at $\sim$1 mm apart. The electrode stripes were perpendicular to the wedge edge coinciding with a thickness gradient. Thus, such a wedge-cell comprised several separate "sub-cells" of

different gap thickness varying in a range from $\sim 2\,\mu m$ to $\sim 18\,\mu m$. We want to mention that with the microscope set-up the measurements for each individual sub-cell were performed for a spot less than 1 mm. At a scale of 1 mm the variation of thickness was of about $0.2\,\mu m$, thus the use of microscope set-up allowed us to minimized the influence of a variable thickness on switching time even for a thinnest sub-cell of a thickness of $2.6\,\mu m$. The average thickness of each sub-cell gap was determined by capacity measurements. The area of each sub-cell was of $\sim 0.2\,cm^2$, and resistance of electrode stripes being of $\sim 150\,\Omega/\square$. The homogeneous planar LC texture was provided by rubbing polyimide alignment layers deposited onto the electrodes of the plates.

Three geometries of LC director orientation (i.e., rubbing direction R of alignment layers) with respect to the direction of the axis P of the input polarizer were used in our experiments: (i) "RP_{45}", when the rubbing direction turned at an angle of 45°; (ii) "RP_0" and "RP_{90}", when the cell rubbing direction is at the angles 0° and 90° respectively. In all the measurements the input and output polarizers were crossed. The electro-optical responses for RP_0 and RP_{90} geometries were not principally different from each other (there was some difference only in amplitudes of optical response). Therefore, below we show only the data for RP_{45} and RP_0 geometries. For RP_{45} geometry, in case of non-twisted LC director field distribution, the time dependent intensity *I(t)* of outgoing light depends on the phase retardation $\Delta\Phi(t)$ of tested cells as:

$$I(t) = I_0 \sin^2\left(\frac{\Delta\Phi(t)}{2}\right), \tag{1}$$

where I_0 is approximately (neglecting reflections and non-ideality of the polarizers) half of the intensity of the incoming nonpolarized light and

$$\Delta\Phi(t) = \frac{2\pi}{\lambda} d\Delta n(t), \tag{2}$$

where $\Delta n(t)$ is an effective birefringence, which has a complicate time dependence defined by a driving voltage waveform and corresponding evolution of the LC director field distribution.

Note right here that for RP_0 and RP_{90} the electro-optical response can be non-zero only if a twist deformation appears in the director field distribution.

3. RESULTS AND DISCUSSION

A. Electro-Optical Response Investigations in Quasi-Static Mode

Figure 5 shows results of quasi-static measurements for the dual-frequency AP-99-1 mixture. The 0-aligned and π-aligned cells of different thickness were investigated. In these figures the normalized transmission-voltage dependencies $T(U) = I(U)/I_0$, which can be described by (1), and the phase retardation $\Delta\Phi(U)$ dependencies extracted in accordance with (1) are shown. The computer simulations of $I(U)/I_0$ dependencies made using specially developed software package (NLCL by P.S.P.) are presented in the same figures. In this software both LC field distribution problem and optical problem are solved using 4×4 matrix method.

The transmission-voltage dependencies are typical of the LC orientational transition from an initial planar LC director field distribution to the homeotropic one. For the cells with the phase retardation $\Delta\Phi$ close to π the initial ($U = 0$) cell transmission has a maximum value (see Fig. 5a). With growing the driving voltage the transmission is decreased and at the high voltage it approaches zero (because $\Delta\Phi \to 0$). For the cells with $\Delta\Phi$ close to 2π the initial cell transmission is minimal (Fig. 5b). With growing the driving voltage the transmission is increased. It passes the maximum at $\Delta\Phi = \pi$ and then decreases, approaching zero at high voltage values (because $\Delta\Phi \to 0$ as well). A residual transmission at high voltages is due to non-reoriented very thin interfacial LC layer regions, those are strongly anchored to the alignment layers. For thick LC layers, when $\Delta\Phi$ is much larger than 2π (Figs. 5c, d), the *I(U)* dependencies have an oscillating character with the extremes of the transmission-voltage curves corresponding to optical phase retardation multiple of π. The $\Delta\Phi(U)$ dependencies (see Figs. 5e, f) show sharp decreasing the phase retardation after the driving voltage has reached the threshold value and then slowly approach zero value (small residual retardation value remains at large driving voltages due to strong anchoring again).

Though the quasi-static response characteristics of 0-aligned and π-aligned cells are practically identical, important peculiarities in a form of slight jumps at $U_{\text{jump}} \sim 5\,\text{V}$ (see Figs. 5a, e) and $\sim 8\,\text{V}$ (see Fig. 5b) are still visible for the π-aligned cells. These slight jumps are well seen in cases of thin cells with a retardation of π and 2π. They occur at certain driving voltages when the director field distribution in middle of the cell gap changes from splay configuration at $U < U_{\text{jump}}$ shown in Figure 6(b) to the "bend" configuration at $U > U_{\text{jump}}$ (Fig. 6(c)).

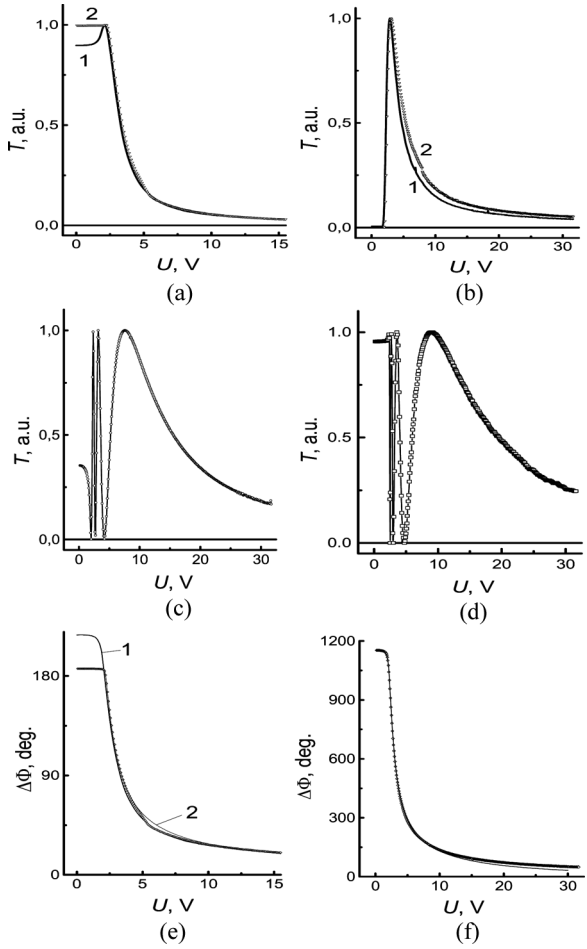

FIGURE 5 The transmission-voltage (a, b, c, d) and optical phase retardation (e, f) versus voltage dependencies for different LC layer thickness and alignment (T = 21°C): (a) and (e) are for 0-alignment at $d = 1.7\,\mu m$ (curves 1) and π-alignment at $d = 1.4\,\mu m$ (curves 2); (b) are for 0-alignment (curve 1) and π-alignment (curve 2) at $d = 2.6\,\mu m$; (c) and (f) are for 0-alignment at $d = 8.1\,\mu m$; (d) is π-alignment at $d = 9.0\,\mu m$. In (e) and (f) the simulated curves (marked with diamond symbols) are also given with the following parameters of modeling: $\Delta\varepsilon = +2.4$, $\Delta n = 0.25$, $\theta = 4^\circ$, $K_{11} = 9.7\,pN$, $K_{33} = 16.5\,pN$, $W_z = 0.5\,mJ/m^2$ and $W_a = 0.05\,mJ/m^2$ (W_z and W_a are zenithal and azimuthal anchoring energies, respectively).

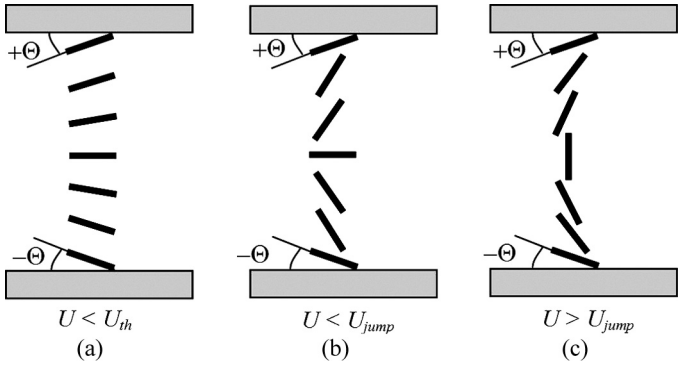

FIGURE 6 Three different configurations of LC director field: nonuniform splay configuration (π-alignment) at $U < U_{th}$ (a), field-on splay configuration at $U < U_{\text{jump}}$ (b), and field-on bend configuration at $U > U_{\text{jump}}$ (c).

The computer simulation with fitting the experimental data (see Figs. 5 e, f) enables us to evaluate some material parameters of the AP-99-1 mixture. In particular, the elastic constants K_{11} and K_{33} for splay and bend deformations respectively were obtained. There is some inaccuracy in K_{11} and K_{33} values obtained for the cells of different thicknesses and alignment conditions (0- or π-alignment), but on average the values of elastic coefficients are as follows: $K_{11} = 9.7\,\text{pN}$, $K_{33} = 16.5\,\text{pN}$.

B. Electro-Optical Response in Dynamic Mode Under Dual-Frequency Driving

Dynamics of the electro-optical response under the cyclic driving for 0-aligned cells with different LC layer thickness (2.6 μm, 5.2 μm, 7.6 μm and 10 μm) is demonstrated in Figure 7. The thicknesses of the layers correspond to field-off phase retardations 2π, 4π, 6π and 8π. The fine adjustment of the field-off initial phase retardation to this values even of π was made in RP_{45} geometry by moving the probing laser beam perpendicular to electrode stripes (i.e., along the wedge direction of the cell) to get a minimum of the transmission. Due to the wedge-like cell the variation of LC layer thickness over the electrode stripe area with respect to the middle width stripe position was of $\sim 0.2\,\mu\text{m}$. The transmission level $T = 1$ corresponds to a maximum value cells provide at odd multiple of π phase retardation. The driving waveform is shown at the bottom of the Figure 7. Both low and high frequency modulated pulses of the driving dual-frequency waveform is of 1 ms in duration. Almost homeotropic distribution of LC director providing the net phase retardation $\Delta\Phi \approx 0$ is reached at low frequency driving pulse of about 50 V.

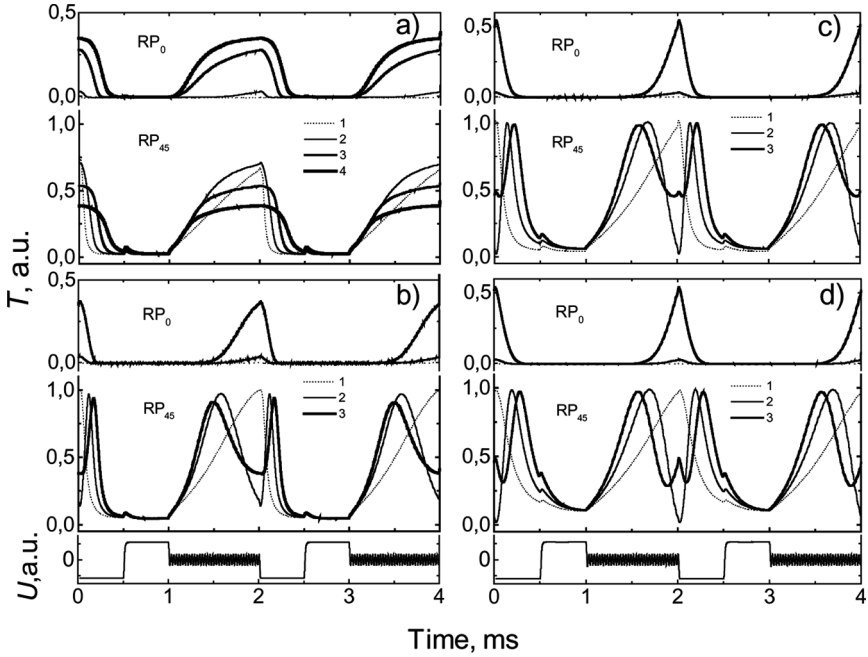

FIGURE 7 Electro-optical response of the 0-aligned AP-99-1 cells measured in RP_0 and RP_{45} geometries at $U_{LF} = 50\,V$ and U_{HF} voltage of different values (T = 22°C). a) $d = 2.6\,\mu m$, curves 1–4 are for U_{HF} equal to 7, 14, 17 and 21 V, respectively; b) $d = 5.2\,\mu m$, curves 1–3 are for U_{HF} equal to 15, 21 and 28 V, respectively; c) $d = 7.6\,\mu m$, curves 1–3 are for U_{HF} equal to 22, 33 and 35 V, respectively; d) $d = 10\,\mu m$, curves 1–3 are for U_{HF} equal to 30, 38 and 44 V, respectively. The lower traces represent the applied voltage waveform.

As seen in Figure 7, in case of RP_{45} geometry a transmission value close to unit corresponding to a phase retardation of π can not be achieved for the cell with 2.6 μm LC layer thickness, despite the layer is capable to provide a phase retardation of 2π in the quasi-static regime. At first glance with increasing the high frequency voltage U_{HF} at a fixed low frequency voltage U_{LF} the LC director field distribution should become closer to the planar state, and the phase retardation have to be increased (*rsm* values of voltages are assumed). However, at exceeding some certain value of U_{HF}, the transmission in RP_{45} geometry begins to fall long before it reaches a maximum value of $T = 1$. At the same instant, the step-wise growth of transmission appears in RP_0 geometry. A non-zero transmission in RP_0 geometry can only be explained if LC director field is subjected to twist

deformation. By additional experiments and numerical simulations we have established that the cause of the observed behavior is due to the back flow effects, which are developed to electrohydrodynamic (EHD) instability at larger high-frequency fields. The EHD is a result of complex hydrodynamics developed in LC layer, when driving voltage exceeds a certain threshold value. The hydrodynamic flows destabilize the in-plane reorientation by creating twist deformation of the LC director field. At voltages higher of threshoulds values, the EHD instability is characterized by appearance of a periodic distortion of LC texture. In RP_0 and RP_{90} geometries the EHD instability looks like striped (black-bright) domains oriented along the rubbing direction. Photo 1(a, c and d) demonstrates images of domains observed in the 0-aligned and π-aligned cells. At further growth of U_{HF},

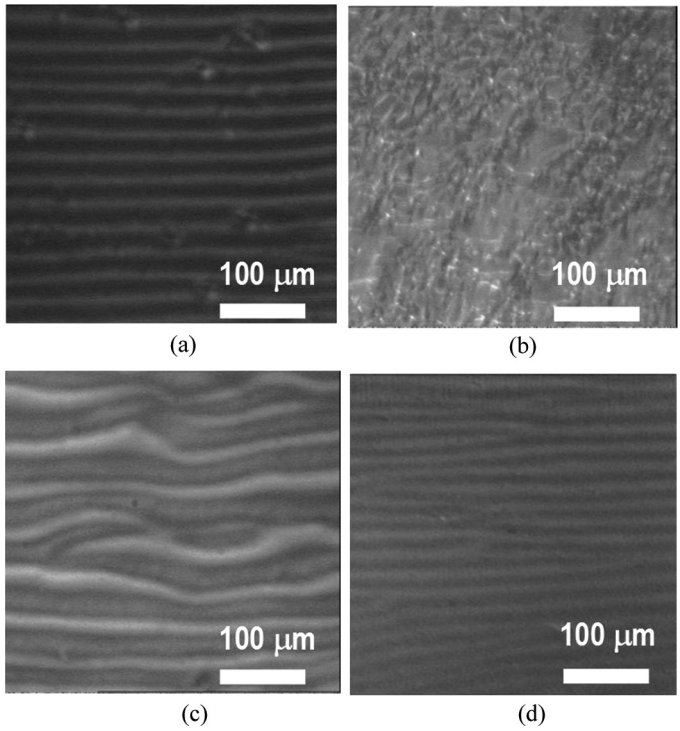

PHOTO 1 The optical patterns of EHD instability for 0- (a, b, c) and π-aligned (d) AP-99-1 cells at $U_{LF} = 50\,V$, $\tau_{HF} = \tau_{LF} = 1\,ms$: a) $-d = 6.3\,\mu m$, $U_{HF} = 35\,V$; b) $-d = 6.3\,\mu m$, $U_{HF} = 42\,V$; c) $-d = 10.3\,\mu m$, $U_{HF} = 57\,V$; d) $-d = 10.7\,\mu m$, $U_{HF} = 50\,V$ ($T = 22^{\circ}C$). The images are taken at crossed polarizers in RP_0 geometry.

regular hydrodynamics flows become turbulent and accompanied by strong light scattering. An image in case of such turbulence is demonstrated by Photo 1b. It is important to mention that an appearance of the EHD instability is not a consequence of the wedge-like shape of the sample. The EHD appears along the rubbing direction independently on either the rubbing is done alone the thickness gradient of the sample or in the perpendicular direction. Also we have checked independently that the EHD instability is observed in "flat" cells as well.

For the π-aligned cells with almost equivalent LC layer thickness values (2.5 μm, 5.6 μm, 7.8 μm and 10 μm) the dynamics of the electro-optical response was also investigated. The electro-optical response for π-aligned cells is only slightly different from one already demonstrated in Figure 7 for 0-aligned cells. Slight distinction is in regards to values of driving voltages. In Figure 8 we summarize the experimental results of thickness dependencies of the high-frequency driving voltage U_{HF} for both 0-aligned and π-aligned cells: i) EHD instability appearance (threshold voltages, curves 1, 2); for stable 2π phase modulation (curves 3, 4); iii) for stable π phase modulation (curves 5, 6). The odd and even curves numbers correspond to the 0- and π-aligned cells, respectively. The low frequency voltage U_{LF} in these experiments is maintained at a constant value of 50 V.

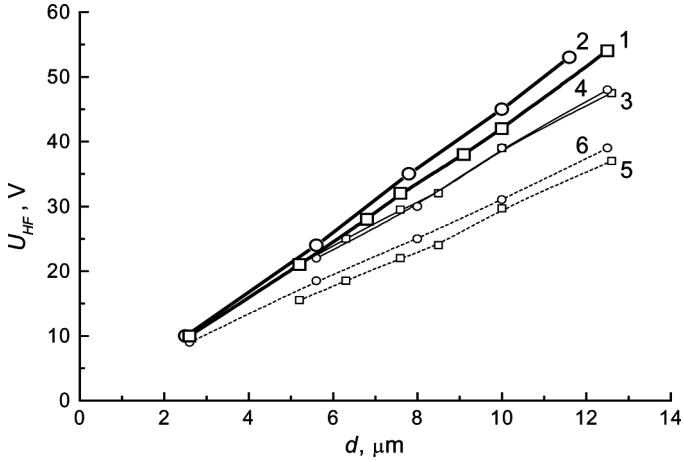

FIGURE 8 Thickness dependence of high frequency (35 kHz) voltage U_{HF} at which a phase retardation of π (5, 6) and 2π (3, 4) is still reached (100% light modulation efficiency is observed). The curves 1 and 2 show approximate dependencies of the threshold voltage of phase modulation breakdown for 0- and π-aligned LC cells, respectively. $U_{LF} = 50$ V, T = 22°C.

The plot area above the curves 1 and 2 corresponds to EHD instability for 0- and π-aligned cells, respectively. As is seen from Figure 8, owing to the EHD instability restrictions the fast (500 Hz) stable 2π phase modulation can only be realized if the LC layer thickness is larger than 7 μm. For thinner LC layers within a range of $3\,\mu m < d < 6\,\mu m$ a maximum phase modulation of π can only be achieved (see curves 5 and 6).

The stable and fast 2π phase modulation is possible at approximately same voltages applied to cells of equal thickness in case of both 0- and π-alignment. However, the voltages for the stable π-phase modulation are still lower for the 0-aligned cells compared to the π-aligned cells. This is a consequence of different space distribution of the back flow velocities across the cell gap thickness. The threshold voltage of the EHD instability is found to be slightly higher for the π-aligned cells compared to the 0-aligned cells (see Fig. 8). Therefore, at equal layer thicknesses and the fixed low-frequency driving, larger phase retardation on π-aligned cells is received. It is important to mention that the stable phase modulation in case of π-aligned cells is established not immediately the driving is switched-on, but after some time interval the transition of the initial splay director configuration (see Fig. 9a) into the bend one (Fig. 9b) occurs. Namely the bend-distorted LC layers provide the stable phase modulation. However, the bend-like director field deformation is topologically nonequivalent to the initial splay configuration. For the last reason after the driving voltage is switched off, the director field relaxes not to the initial splay configuration, but to a topologically equivalent 180°-twisted configuration (Fig. 9c). This 180°-twisted director configuration very slowly

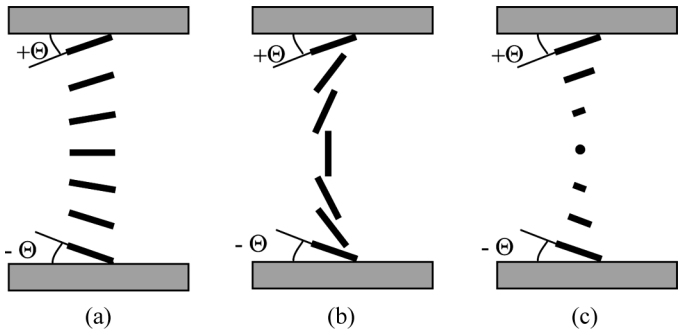

FIGURE 9 The configuration of LC director: π-alignment (splay configuration) before voltage applied (a), bend configuration under voltage-on (b), 180°-twist after voltage-off (c).

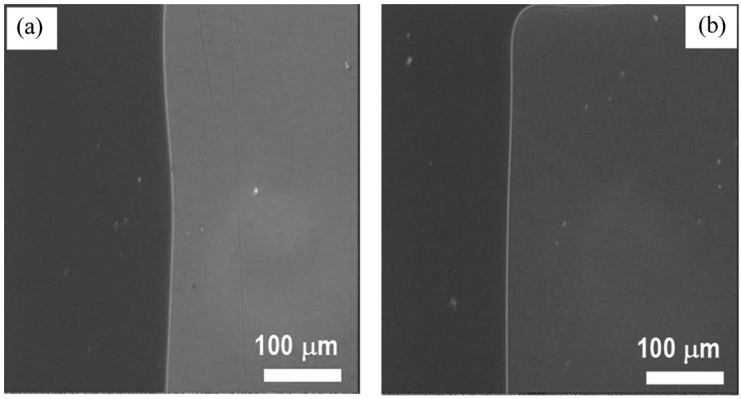

PHOTO 2 An image of two domains observed for PR_0 geometry in AP-99-1 π-aligned cells of $d = 5.6$ (a) and 8 μm (b), after the driving voltage is switched-off. The brighter domains correspond to 180°-twisted director configurations, the darker domains are for the initial splay director configuration.

relaxes to the initial splayed state due to topological nonequivalence of these two states (actually, the transition appears because of presence of defects and thermal fluctuations). Photo 2 shows texture images taken in PR_0 geometry for the π-aligned cell after the driving voltage is switched-off. Two different domains are clearly seen during the relaxation. On each picture a brighter domain corresponds to the 180°-twisted director configuration, while in the darker domain the director field distribution corresponds to planar and thermodynamically stable splay configuration. Note, that the transition into the 180°-twisted director configuration is a result not only of the dual-frequency mode of switching. For instance, such a transition takes place during the free relaxation each time after the splay director configuration is transformed into the bend configuration under the single low frequency pulses driving too. The bend configuration appears if the low frequency voltage pulse amplitude and duration are sufficient to destroy a middle-layer "wall" with a planar director orientation characteristic of splay cells.

Both the high frequency voltages U_{HF}, at which phase retardations of π and 2π and EHD threshold are reached, grow linearly with increasing of the LC layer thickness d. However, the EHD threshold voltage dependence has a higher derivative. Owing to this, as the LC layer thickness is increased, it is possible to realize the stable modulation with a higher phase retardation. For instance, at $d = 12.5$ μm a stable modulation of $\sim 3\pi$ can be reached, while at $d < 5.5$ μm even the 2π

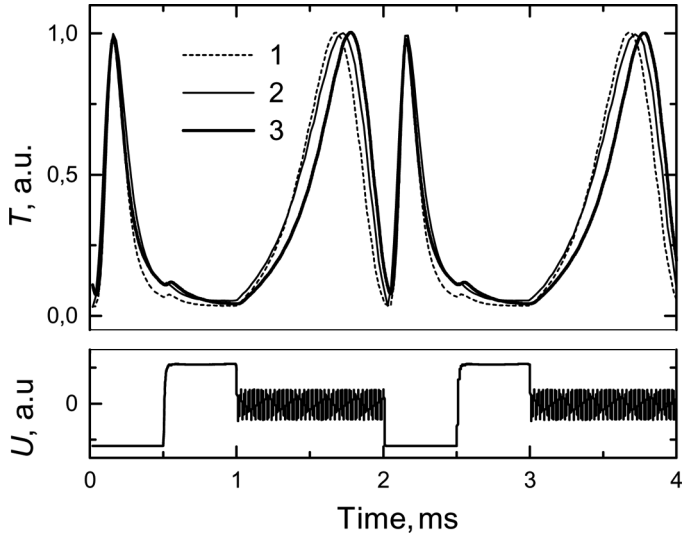

FIGURE 10 Electro-optical response in regime of 2π-phase retardation switching for the 0-aligned AP-99-1 cell of three different thicknesses of LC layer (T = 23°C): 1–$d = 7.6\,\mu$m, $U_{LF} = 50\,$V, $U_{HF} = 30\,$V; 2–$d = 10.3\,\mu$m, $U_{LF} = 60\,$V, $U_{HF} = 41\,$V; 3–d = 12.5 μm $U_{LF} = 70\,$V, $U_{HF} = 48\,$V. The lower trace represents the applied voltage waveform (Remark. The modulation, which is visible on high frequency trace on this and others figures is an apparent effect, caused by insufficient data sampling frequency when the oscilloscope is set to a given time resolution).

modulation is impossible with the same switching time. However, at larger LC layer thicknesses the higher voltage amplitudes are required to reorient LC layer into homeotropic state ($\Delta\Phi \approx 0$) and to get comparable switching time. All this is demonstrated in Figure 10, which shows the electro-optical response in regime of the 2π phase retardation switching for three different thicknesses of LC layer: 7.6 μm, 10.3 μm and 12.5 μm. At $d = 7.6\,\mu$m, phase retardation switching from 0 to 2π is realized during a time τ_{on} of 1 ms at $U_{HF} = 30\,$V. In this case $U_{LF} = 50\,$V is sufficient to switch the phase retardation from $\Delta\Phi \approx 2\pi$ to $\Delta\Phi \approx 0$ during time less than 1 ms. At $d = 12.5\,\mu$m the corresponding voltages are: $U_{HF} = 48\,$V and $U_{LF} = 70\,$V.

The phase retardation switching times for both low and high-frequency driving pulses are controlled by cell thickness d and the driving voltage U. Switching times τ_{on} depend inversely on the electric field strength, $\tau_{on} \sim d/U = 1/E$, but not as $\sim 1/E^2$. This can be seen from examination of the electro-optic response records in Figure 10.

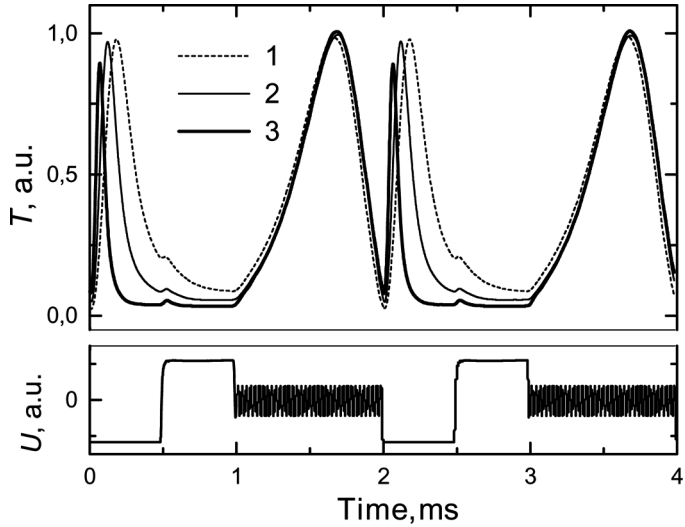

FIGURE 11 Electro-optical response in regime of 2π-phase switching for 0-aligned cells of 7.7 μm in thickness for different low frequency voltage U_{LF} at fixed $U_{HF} = 30\,\text{V}$ (T = 23°C): $1 - U_{LF} = 30\,\text{V}$; $2 - U_{LF} = 50\,\text{V}$; $3 - U_{LF} = 80\,\text{V}$. The lower traces represent the waveform of applied voltage.

Indeed, d, U_{LF} and U_{HF} values, at which phase retardation of π and 2π is reached, are related to each other by the direct proportionality. The phase retardation switching times in cases of the π-aligned cells are close to those for 0-aligned cells.

The EHD instability is not induced if the LC cell is subjected only to either a low frequency (1 kHz) or high frequency (35 kHz) driving voltage. The EHD instability is a consequence of applying to the LC cell of the periodic dual-frequency driving pulses. We can also state that the high frequency driving pulses play a key role in appearance of EHD instability. This is demonstrated in Figure 11, where electro-optical responses of 0-aligned cell is shown for fixed value of high frequency pulse U_{HF}, while low frequency driving pulse value U_{LF} are varied from 30 V to 80 V. It is seen, that increasing U_{LF} decreases the time of phase retardation switching to $\Delta\Phi \sim 0$, but it does not result in destabilizing the phase modulation. The cell transmission in RP_0 geometry is practically unchanged (in Fig. 11 it is not shown). However, the value of U_{HF} influences critically on the phase modulation behavior for both 0- and π-aligned cells (see, as example, Fig. 7 for 0-aligned cells).

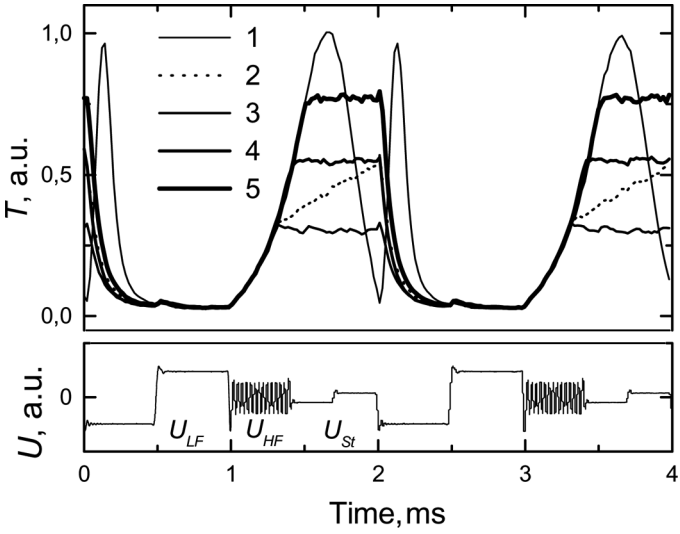

FIGURE 12 Temporal behaviour of the electro-optical response of the 0-aligned AP-99-1 cell ($d = 7.6\,\mu m$) upon high frequency pulse durations τ_{HF} and stabilization of the phase retardation on some values using low-frequency voltage $U_{St} \cdot U_{LF} = 50\,V$ ($\tau_{LF} = 1\,ms$) and $U_{HF} = 30\,V$ (T = 22°C): $1 - \tau_{HF} = 1\,ms$; $2 - \tau_{HF} = 0.3\,ms$, $U_{St} = 0\,V$; $3 - \tau_{HF} = 0.3\,ms$, $U_{St} = 18\,V$; 4-$\tau_{HF} = 0.4\,ms$, $U_{St} = 10\,V$; $5 - \tau_{HF} = 0.5\,ms$, $U_{St} = 7\,V$.

Switching of phase retardation from 0, which is set by low frequency pulse, to any other value can be realized at fixed-amplitude high-frequency pulses of variable duration τ_{HF} as shown in Figure 12. In this version of the phase retardation switching time for different $\Delta\Phi$ values is controlled by the duration of the high frequency pulse. After the high frequency driving pulse is switched-off, the phase retardation value is changed with time, because of a free LC director relaxation to the initial planar configuration (curve 2 in Fig. 12). By applying a certain low frequency voltage (2 kHz square wave was used) just after ending the high frequency pulse one can stabilize the phase retardation on a desired value (curves 3–5 in Fig. 12). The value of stabilizing voltage (U_{St}) depends on the director field distortion, which takes place at a desired $\Delta\Phi$ level. The closer the director orientation to the homeotropic one, the larger U_{St} value is needed. Of course, the control of a phase retardation value can also be done by variations of both low- and high-frequency voltage parameters. Two of possible scenarios of settings different retardation values in range between 0 and 2π are illustrated in Figure 13.

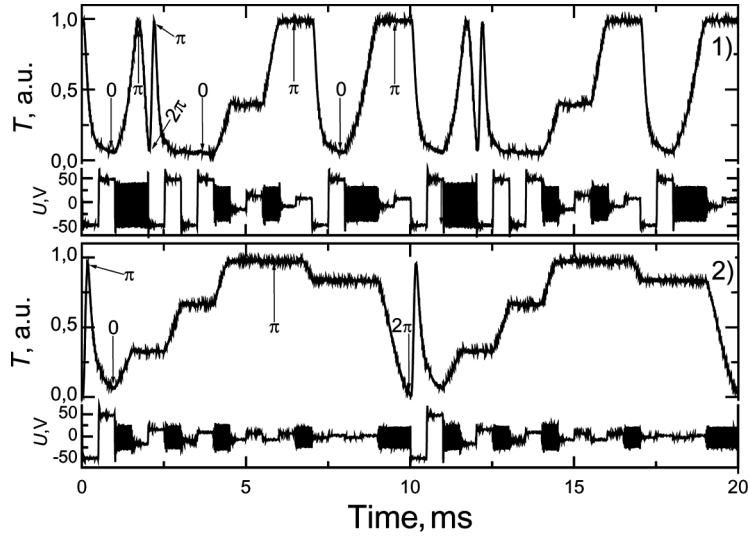

FIGURE 13 Two scenarios (1, 2) of optical phase retardation switching within the range from 0 to 2π for the 0-aligned AP-99-1 cell of thickness $d = 7.7\,\mu m$ ($T = 22^{\circ}C$). The phase retardation values $\Delta\Phi = 0$, π and 2π are pointed by the arrows. The lower traces represent the waveform of applied voltage.

4. CONCLUSION

To conclude, we have performed the study of general features of the optical phase retardation switching in dual-frequency liquid crystals. The phase retardation characteristics for both 0-aligned and π-aligned cells were investigated under the quasi-static and dynamic electric field control. We have established that the main obstacle in development of dual-frequency liquid crystal modulators of high phase-retardation values appears from EHD instability that destabilizes the non-twisted director reorientation. The general conclusions related to the EHD role have been confirmed by both experiments on different kinds of dual-frequency materials and by numerical simulations. The most typical results were illustrated on the developed dual-frequency liquid crystal material AP-99-1, which possesses sign inversion of dielectric anisotropy at 9 kHz ($T = 21^{\circ}C$). The stable switching of phase retardation for any desired value within dynamic range of 2π at switching time of less than 2 ms was obtained for a layer thicknesses larger than 7 μm of the developed dual-frequency liquid crystal material at room temperature. To obtain such phase

modulation parameters for layer thicknesses as large as 8 μm, the driving voltages of 50 V and 30 V at low (1 kHz) and high (35 kHz) frequencies respectively are sufficient.

Both 0-aligned and π-aligned LC layers can be used for 2f-LCM based phase modulators. However, for the stable phase modulation regime of π-aligned cells to be set, the initial splay director configuration should be transferred into the bend one. This bend director configuration, when driving voltage is switched off relaxes inevitably into a 180°-twisted director configuration, which then transforms slowly to the initial splay director configuration owing to the presence of defects and thermal fluctuations.

REFERENCES

[1] Basov, N. G., Berezin, P. D., Blinov, L. M., Kompanets, I. N., Morozov, V. N., & Nikitin, V. V. (1972). *Pis'ma v ZhETF*, *15*, 200, (in Russian).
[2] Vasil'ev, A. A., Kompanets, I. N., & Parfenov, A. V. (1983). *Sov. J. Quantum Electron*, *13*, 689.
[3] Vasil'ev, A. A., Naumov, A. A., & Shmal'gauzen, V. I. (1986). *Sov. J. Quantum Electron.*, *16*, 471.
[4] Dou, R. & Giles, M. K. (1995). *Opt. Lett.*, *20*, 1583.
[5] Baier-Saip, J. A., Bostanjoglo, O., Eichler, H. J., & Macdonald, R. (1995). *J. Appl. Phys.*, *78*, 3020.
[6] McManamon, P. F., Dorschner, T. A., Corcum, D. L., Friedman, L. J., Hobbs, D. S., Holz, M., Liberman, S., Nguyen, H. Q., Resler, D. P., Sharp, R. C., & Watson, E. A. (1996). *Proc. IEEE*, *84*, 268.
[7] Love, G. (1997). *Appl. Opt.*, *36*, 1517.
[8] Dayton, D. C., Browne, S. L., Sandven, S. P., Gonglewski, J. D., & Kudryashov, A. V. (1998). *Appl. Opt.*, *37*, 5579.
[9] Kelly, T.-L. & Love, G. D. (1999). *Appl. Opt.*, *38*, 1986.
[10] Vorontsov, M. A. (1999). *J. Opt. Soc. Am. A*, *16*, 2567.
[11] Restaino, S. R., Dayton, D., Browne, S., Gomglewski, J., Baker, J., Rogers, S., McDermott, S., Gallegos, J., & Shilko, M. (2000). *Opt. Express*, *6*, 2.
[12] Love, G. D. (1993). *App. Opt.*, *36*, 1517.
[13] Pan, C.-L., Huang, M., & Pan, R.-P. (2004). *Mol. Cryst. Liq. Cryst.*, *413*, 561.
[14] Martinez, T., Wick, D. V., & Restaino, S. R. (2001). *Opt. Express*, *8*, 555.
[15] Bucher, H. K., Klingbiel, R. T., & Van Meter, J. P. (1974). *Appl. Phys. Lett.*, *25*, 186.
[16] Raynes, E. P. & Shanks, J. A. (1974). *Electr. Lett.*, *10*, 114.
[17] De Jeu, W. H., Gerittsma, G. J., Van Zanten, P., & Goossens, W. Y. A. (1972). *Phys. Lett.*, *39 A*, 355.
[18] Gerittsma, G. J., de Klerk, J. J. M. J., & Van Zanten, P. (1975). *Sol. State Comm.*, *17*, 1077.
[19] Bak, C. S., Ko, K., & Lobes, M. M. (1975). *J. Appl. Phys.*, *46*, 1.
[20] Barnik, M. I., Ivashchenko, A. V., Kostilev, K. A., Malofeev, B. C., & Shtykov, N. M. (1980). *Opt.-Mechanicheskaya Promishlennost'*, *5*, 25, (in Russian).
[21] Restaino, S. R., Dayton, D., Browne, S., Gomglewski, J., Baker, J., Rogers, S., McDermott, S., Gallegos, J., & Shilko, M. (2000). *Opt. Express*, *6*, 2.

[22] Dayton, D., Browne, S., Gonglewski, J., & Resaino, S. (2001). *Appl. Opt.*, *40*(15), 2345.
[23] Kirby, A. K. & Love, G. D. (2004). *Opt. Express*, *12*, 1470.
[24] Fan, Y.-H., Ren, H., Liang, X., Lin, Y.-H., & Wu, S.-T. (2004). *Appl. Phys. Lett.*, *85*, 2451.
[25] Lu, Y.-Q., Liang, X., Wu, Y.-H., Du, F., & Wu, S.-T. (2004). *Appl. Phys. Lett.*, *85*, 3354.
[26] Liang, X., Lu, Y.-Q., Wu, Y.-H., Du, F., Wang, H.-Y., & Wu, S.-T. (2005). *Jap. J. Appl. Phys.*, *44*, 1292.
[27] Golovin, A. B., Shiyanovskii, S. V., & Lavrentovich, O. D. (2003). *SID'03 DIGEST*, 1472.
[28] Yin, Y., Gu, M., Golovin, A. B., Shiyanovskii, S. V., & Lavrentovich, O. D. (2004). *Mol. Cryst. Liq. Cryst.*, *421*, 133.
[29] Jewel, S. A., Taphouse, T. S., & Sambels, J. R. (2005). *APL*, *87*, 021106.
[30] Jewel, S. A. & Sambles, J. R. (2006). *Phys. Rev E*, *73*, 011706.
[31] Barnik, M. I., Blinov, L. M., Ivashchenko, A. V., & Shtykov, N. M. (1979). *Crystallography*, *24*, 811, (in Russian).
[32] Barnik, M. I., Lazarev, V. V., Maltzev, E. E., & Shtykov, N. M. (1996). *Mol. Mat.*, *6*, 129.
[33] Palto, S., Barberi, R., Iovane, M., Lazarev, V. V., & Blinov, L. M. (1999). *Mol. Mat.*, *11*, 277.